MIT Libraries | DSpace@MIT

MIT Open Access Articles

Low Energy Nanoemulsions as Templates for the Formulation of Hydrophobic Drugs

The MIT Faculty has made this article openly available. ***Please share*** how this access benefits you. Your story matters.

Citation: Badruddoza, Abu Zayed Md, Gupta, Ankur, Myerson, Allan S., Trout, Bernhardt L. and Doyle, Patrick S. 2018. "Low Energy Nanoemulsions as Templates for the Formulation of Hydrophobic Drugs." Advanced Therapeutics, 1 (1).

As Published: http://dx.doi.org/10.1002/adtp.201700020

Publisher: Wiley

Persistent URL: https://hdl.handle.net/1721.1/140464

Version: Author's final manuscript: final author's manuscript post peer review, without publisher's formatting or copy editing

Terms of use: Creative Commons Attribution-Noncommercial-Share Alike

Massachusetts Institute of Technology

Low Energy Nanoemulsions as Templates for the Formulation of Hydrophobic Drugs

Abu Zayed Md Badruddoza *[1], Ankur Gupta *[2], Allan S. Myerson[1], Bernhardt L. Trout[1], and Patrick S. Doyle †[1]

[1]Massachusetts Institute of Technology, Department of Chemical Engineering, Cambridge, MA, 02139 United States
[2]Princeton University, Department of Mechanical and Aerospace Engineering, Princeton, NJ 08540 United States

December 1, 2017

Author Manuscript

Abstract

Most small molecule active pharmaceutical ingredients (APIs) are hydrophobic which poses formulation challenges due to their poor water solubility. Current approaches are energy-intensive and involve presenting the API in a nanoparticle form that is then combined with other additives into a stable formulation. Here, we present a bottom-up and scalable method that formulates nanoparticles (crystalline or amorphous) of poorly water-soluble APIs directly embedded in composite hydrogel beads. Using nanoemulsions prepared from a low energy method as templates, our flexible approach allows us to vary the embedded API nanoparticle size from 100 to 500 nm and the hydrogel bead size from 100 μm to 1200 μm, and subsequently achieve control over the dissolution kinetics. To better understand the dissolution process, we build a physical model that allows us to collapse the kinetic data onto a master curve and predict the dependence of release rates on size of both API nanoparticles and hydrogel beads. Lastly, we demonstrate that we can tune the dissolution kinetics of multiple drugs embedded in the same hydrogel matrix simultaneously, an attractive property for commercial multi-drug dosage applications. The new approach not only leads to process intensification, but also improved performance.
Keyword: nanoemulsions, formulation, nanocrystals, dissolution, controlled release, fenofibrate, ibuprofen

1 Introduction

Estimates suggest that approximately 70% of newly discovered drug candidates and 40% of the marketed immediate release oral drugs have poor aqueous solubility, many of which are categorized as practically insoluble (<100 μg/mL) [1]. Limited aqueous solubility of these drugs poses a challenge to develop formulations. Further, their delivery through an oral route is difficult due to poor and variable bioavailability. Over the past decade or so, several strategies have been proposed to tackle these challenges, such as particle-size diminution, emulsion (micro/ nano) based formulations, self-emulsifying systems, salt formation, micronization, liposomes, micelle formation, cyclodextrin inclusion complexation, and solid dispersions. [2–8]

Nanonization (media milling, nanoemulsions, polymeric micelles) is a common approach to overcome the poor bioavailability of hydrophobic drugs. Nanoemulsions, *i.e.* emulsions with droplet size ranging from 10-500 nm, enhance the permeability and bioavailability of poorly water-soluble drugs by improving drug absorption both orally and topically [9–14]. Nanoemulsion synthesis can be divided into two categories: high energy and low energy methods [11, 13–17]. High-energy methods such as high-pressure homogenization and ultrasonication are brute-force techniques that use excess shear to breakup droplets into sub-micron sizes. These methods require energy on the order of 10^7 - 10^9 W/kg that limits their utility at an industrial scale [11, 15, 16]. In contrast, low energy methods

*equal contribution
†corresponding author, email: pdoyle@mit.edu

This is the author manuscript accepted for publication and has undergone full peer review but has not been through the copyediting, typesetting, pagination and proofreading process, which may lead to differences between this version and the Version of Record. Please cite this article as doi: /adtp.201700020

This article is protected by copyright. All rights reserved.

exploit favorable interfacial properties and require significantly less energy input of about 10^3- 10^5 W/kg, providing an easy and scalable route [11]. Recently, we developed a general route to prepare nanoemulsions using low energy methods where we showed that to make nanoemulsions, depending on the interaction of surfactant(s) with liquid phases, a specific mixing order is required [18]. Due to stability issues, it is preferred to convert the nanoemulsion into a nanoparticle.

Several prior works encapsulate oil nanodroplets containing hydrophobic API inside a hydrogel [19–21], and some of them also solidify API to make nanocrystals by evaporating the oil phase [22, 23]. These studies report enhanced dissolution rate, improved bioavailability of lipophilic compounds, and controlled release of water-insoluble molecules within the human gastrointestinal tract. Engineered hydrogels containing solid API particles and excipient(s) are of industrial interest since they can provide tailored dosage and release profiles [22–24], and also enable intensification (and simplification) of the traditional pharmaceutical manufacturing processes [25–27]. In particular, the latter is possible since solidified API laden composite hydrogels can be directly integrated into customized solid dosage forms, *i.e.* tablets and capsules. However, the aforementioned studies used high energy methods to generate nanoemulsions and are not favorable for industrial scale up. Moreover, they currently lack a quantitative understanding of parameters that control release patterns and rely on phenomenological, power-law, and semi-quantitative transport models [23, 28, 29]. Lastly, prior studies do not provide a route to include multiple drugs in a single gel matrix, an important feature for solid dosage forms.

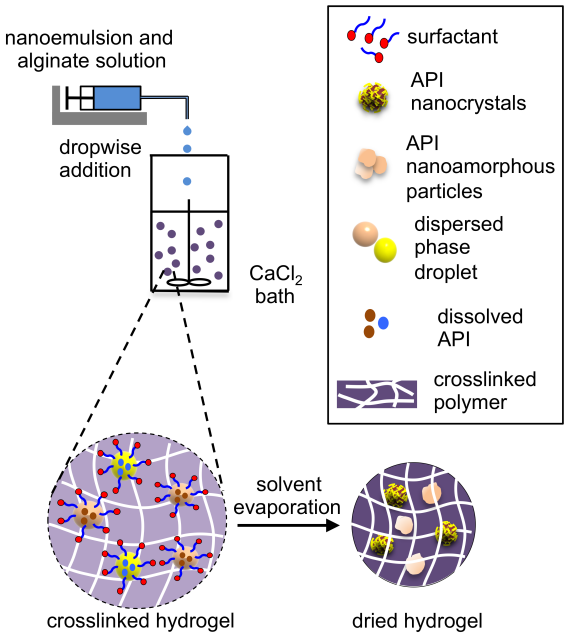

Figure 1: **Schematic of setup for formulation of hydrophobic API.** Nanoemulsions are prepared with a mixture of anisole containing a soluble hydrophobic API as dispersed phase, and aqueous alginate solution as continuous phase. The alginate nanoemulsion solution is dripped into a $CaCl_2$ bath where ionic crosslinking of alginate creates a gel network that traps the nanoemulsion droplets containing the soluble API. Subsequent evaporation of the solvents generates hydrogel beads with API nanocrystals or amorphous nanoparticles embedded within the polymer matrix. Co-formulation, i.e. combining multiple drugs in a single formulation, is prepared by mixing nanoemulsion solutions containing different API prior to the bead generation step.

In this article, we develop a novel formulation strategy for poorly water-soluble drugs by incorporating low energy nanoemulsions into a biocompatible alginate hydrogel matrix taking the form of a composite microgel particle. Fig.1 summarizes our overall experimental strategy. We use nanoemulsions prepared using our general low energy method [18] as templates to create nanoparticles of two poorly water-soluble model APIs: fenofibrate and ibuprofen. Fenofibrate (FEN) and ibuprofen (IBU) are chosen as model compounds in this study because of their poor aqueous solubility. Both APIs are relatively lipophilic (Class II in Biopharmaceutics Classification System, log $P = 4.0$ (IBU) and log $P = 5.3$ (FEN)) with very poor water solubility (0.0008 mg/ mL and 0.021 mg/mL at 25 °C for FEN and

This article is protected by copyright. All rights reserved.

Author Manuscript

IBU, respectively) [30, 31]. The alginate nanoemulsion solution consists of anisole containing saturated amount of fenofibrate or ibuprofen as the oil (dispersed) phase, and an aqueous solution containing 2 wt% sodium alginate as the continuous phase. The nanoemulsion mixture is dripped into a bath of $CaCl_2$ solution that crosslinks alginate due to the presence of Ca^{2+} ions and traps nanoemulsion droplets containing APIs. Subsequent evaporation of the both water and oil phases generates hydrogel beads with API nanoparticles either in crystalline or amorphous form embedded within the polymer matrix. We characterize the physicochemical properties of nanoemulsions and embedded API nanoparticles by dynamic light scattering (DLS), powder X-ray diffraction (PXRD), differential scanning calorimetry (DSC) and scanning electron microscopy (SEM). We further demonstrate a multi-length scale control over the dissolution kinetics since we independently control the size of both API nanoparticles and hydrogel beads. We also build a physical model and perform an order of magnitude analysis to identify the mechanism of API release from hydrogel beads. This model helps us understand the effect of nanoparticle size and hydrogel bead size on the *in vitro* dissolution profiles. To our knowledge, this is the first demonstration of a low energy method that uses nanoemulsions as templates to reliably control dissolution profiles of hydrophobic APIs. Moreover, our model is useful to understand the dissolution process and set design parameters.

2 Materials and Methods

2.1 Materials

Non-ionic surfactant (Span 80 and Tween 80), fenofibrate (>99% pure), anisole (methoxybenzene, >99% pure), calcium chloride (>93% pure), ibuprofen (>99%) and sodium dodecyl sulfate (>99% pure) are products from Sigma-Aldrich. Sodium alginate (CAS no. 9005383), a polysaccharide that consists of approximately 61% mannuronic (M) and 39% guluronic (G) acid is also purchased from Sigma-Aldrich. 30, 22 and 15 gauge needles are purchased from Nordson EFD. All chemicals or products are used without further purification. DI water is used throughout the experiments.

2.2 Nanoemulsion preparation and characterization

Low-energy alginate nanoemulsions were prepared using a magnetic stirrer for approximately 10 minutes at 1000 rpm and 25 °C by two experimental procedures: method A - adding dispersed phase to a mixture of continuous phase and surfactant, method B - adding continuous phase to a mixture of dispersed phase and surfactant (method B) [18]. Anisole containing a saturated concentration of fenofibrate or ibuprofen is used as the dispersed (oil) phase, and 2% w/v sodium alginate solution is used as the continuous phase. The saturation concentrations of fenofibrate and ibuprofen in anisole are approximately 450 mg/mL and 200 mg/mL, respectively. The composition of the nanoemulsion solution prepared is: $\frac{30}{\text{SOR}+1}$ wt% oil phase - $\frac{30\text{SOR}}{\text{SOR}+1}$ wt% surfactant - 70 wt% alginate aqueous phase. We examine variation of average droplet size (d) for different hydrophile-lipophile balance (HLB) and surfactant-to-oil ratios (SOR). We vary HLB values by mixing non-ionic surfactants Span 80 and Tween 80 in different proportions. The HLB value for a mixture of Tween-80 and Span-80 can be calculated by HLB= 4.3(x) + 15(1 - x), where x is the weight fraction of Span 80 in the mixture. A HLB value of 4.3 (pure Span 80) represents an oleophilic surfactant whereas a HLB value of 15 (pure Tween 80) represents a hydrophilic surfactant. We change SOR values by simply using different relative amounts of oil and surfactant.

Nanoemulsion droplet sizes are measured using dynamic light scattering (DLS). Each measurement sample is prepared by diluting 50 μL of nanoemulsion solution in 4 mL of DI water. The measurement sample is then used for dynamic light scattering (Brookhaven 90Plus PALS, 3 measurements of 2 minutes each) at room temperature. We avoid Ostwald ripening effect since DLS is performed immediately after nanoemulsion preparation. Average diameter (d) and polydispersity are extracted from raw DLS data through second-order cumulant analysis. We observe maximal errors of ±5% for d and ±10% for polydispersity.

2.3 Preparation of hydrogel beads with embedded API nanoparticles

Nanoemulsion-laden composite hydrogel beads are prepared by both dripping and centrifugal methods (centrifugal method is detailed in our previous work [32]). Uncrosslinked alginate nanoemulsion contained in a 5 mL syringe is dripped using gravity or centrifugal force in a drop-wise fashion through a certain sized nozzle into a $CaCl_2$ solution (6 %w/v). Upon contact with $CaCl_2$, alginate crosslinks generating spherical beads that trap the nanoemulsion

This article is protected by copyright. All rights reserved.

Author Manuscript

droplets containing the APIs inside the polymeric network. The beads are then washed with water several times and dried in an oven at 60°C for 2-4 days. During drying, evaporation of both solvents (anisole and water) leads to formation of hydrogel particles with API nanoparticles embedded inside the polymer matrix. The sizes of dried hydrogel beads range from 100 to 1200 μm depending on the syringe-nozzle size. For example, 30 gauge and 15 gauge stainless steel blunt-tip needles are used using gravity dripping to prepare around 650 and 1200 μm sized dried hydrogel beads, respectively. However, to produce < 450 μm sized beads, centrifugal synthesis is used (the preparation method is described in the Supporting Information).

To prepare the co-formulated APIs inside a hydrogel bead, two separate nanoemulsion solutions are mixed in 1:1 ratio by weight. The first nanoemulsion solution is 20 wt% anisole containing saturated amount of ibuprofen - 10 wt% surfactant (HLB 14.3) - 70 wt% alginate solution (SOR= 0.5, nanoemulsion size ∼140 nm) and the second solution is 20 wt% anisole containing a saturated amount of fenofibrate - 10 wt% surfactant (HLB 15) - 70 wt% alginate solution (SOR= 0.5, nanoemulsion size ∼ 520 nm).

2.4 Analysis of hydrogels beads containing drug nanoparticles

The dried composite hydrogel beads with fenofibrate or ibuprofen nanoparticles embedded inside the polymer core matrix are analyzed by powder X-ray diffraction (PXRD) in reflectance mode (Panalytical X'pert MPD Pro). The samples are ground and then placed on a zero background disk. The PXRD is operated at 40 kV, 30 mA, and at a scanning rate of 2°/min over the range of 2θ = 10 - 40°, using Cu-Kα radiation wavelength of 1.54 $\AA$. The samples are also analyzed by differential scanning calorimetry (DSC) using TA Instruments (Q2000 DSC). 10 - 15 mg of sample is crimped in a sealed T-zero aluminum pan and heated at 10 °C/min in the range of -20 °C to 150 °C using an empty sealed pan as a reference. Dry N_2 is used as purge gas and the flow rate is 50 mL/min. The embedded API nanoparticles are also characterized with high-resolution scanning electron microscope (Zeiss HRSEM) at 5 kV accelerating voltage and at various magnifications. Prior to imaging, all samples are prepared on conventional SEM stubs with carbon tape and are coated with about 10-15 nm of Au by sputter coating.

2.5 Dissolution experiments

The *in vitro* dissolution of fenofibrate and ibuprofen from the composite hydrogel beads is carried out using the standard USP II (paddle) apparatus at 37 °C and 75 rpm. The dissolution media used in these experiments is 900 mL of water containing 0.72% w/v SDS for fenofibrate and 900 mL of 0.2 M Na-phosphate buffer (pH 7.0) for ibuprofen. The samples of dried composite hydrogel formulation (equivalent to about 20 mg of API) are added to the dissolution media manually. To maintaining sink conditions during dissolution experiments, the mass of drugs added for a dissolution experiment is at least 3 times less than the amount required to saturate the media. The UV measurements are obtained using an automatic Varian UV-vis Cary 50 apparatus and an *in situ* probe set. All reported measurements are repeated at least 3 times under identical conditions to obtain an average value.

3 Results and Discussion

3.1 Characterization of API nanoparticles

We first discuss and characterize the results of optimal nanoemulsion formulations with ibuprofen and fenofibrate individually. Controlling the emulsion droplet size is crucial in emulsion-based formulation since the confined environment of droplet dictates the drug particle attributes (size, shape). We show in our previous work that fenofibrate crystal size is dictated by the nanoemulsion droplet size, which subsequently influences the dissolution kinetics [22, 23]. Fig.2 shows the variation of nanoemulsion droplet size with formulation parameters such as the order of mixing of different phases (method A or method B), hydrophile-lipophile balance (HLB) of surfactants and surfactant-to-oil ratio (SOR). The composition of the nanoemulsion solution is: $\frac{30}{\text{SOR}+1}$ wt% oil phase (anisole containing saturated amount of API) - $\frac{30\text{SOR}}{\text{SOR}+1}$ wt% surfactant - 70 wt% alginate aqueous phase. We examine the variation of droplet size with HLB (HLB of a surfactant estimates the relative interaction of the surfactant with the liquid phases). We also vary SOR to see the range of accessible compositions since that ultimately dictates the scalability of the process. It is seen from Fig.2 (a)) that the average droplet size decreases with increase in HLB for both methods A and B, and for both hydrophobic APIs. We also observe that method A yields lower droplet sizes when compared

This article is protected by copyright. All rights reserved.
Author Manuscript

with method B, consistent with results from previous work [18]. HLB is thus a useful parameter and can be used to control the droplet size. We note that HLB range can be extended further by using different surfactant(s). We refer the readers to our recent work for more strategies to tune the droplet size through choice of surfactant, mixing order, and composition [18]. Increase in SOR also decreases droplet size for both method A and B, and for both APIs (Fig.2 (b)). This is also consistent with expectation since increasing the relative amount of surfactant improves the surfactant migration to nanoemulsion interface, leading to a more effective droplet breakup. Since even low SORs (such as SOR=0.25) enable efficient nanoemulsion formation, we can achieve high drug loading capacities (see Supporting Information for more details). Thus, our methodology has a high potential for scale up.

We investigate the crystallinity of encapsulated API nanoparticles inside the hydrogel matrix by powder X-ray

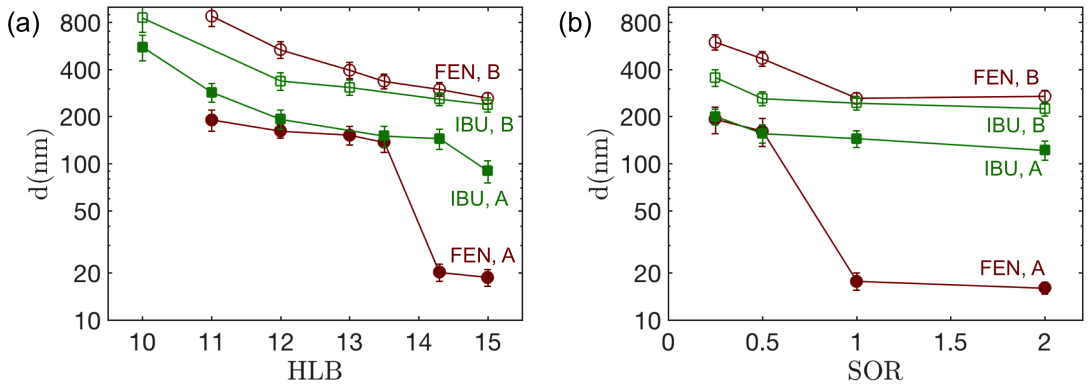

Figure 2: **Summary of average nanoemulsion droplet size with a mixture of anisole containing soluble hydrophobic API as dispersed phase and aqueous alginate solution as continuous phase.** (a) Variation of average droplet size d with HLB of surfactants for methods A / B using either fenofibrate (FEN) or ibuprofen (IBU) as a model API. d decreases with increase in HLB for both methods and for both APIs. Moreover, method A is superior to method B for all HLB values. SOR=1 is kept constant and HLB value is varied by using a mixture of Span 80 (HLB=4.3) and Tween 80 (HLB=15). (b) Variation of average droplet size d with surfactant-to-oil ratio SOR. d decreases with increase in SOR for both methods and for both APIs. Here also, method A is superior to method B for all SOR values. HLB=14.3 is kept constant. The composition of nanoemulsion used is $\frac{30}{\text{SOR}+1}$ wt% oil phase (anisole containing saturated amount of API) - $\frac{30\text{SOR}}{\text{SOR}+1}$ wt% surfactant - 70 wt% alginate aqueous phase. Error bars represent variation in polydispersity.

diffraction (PXRD) and differential scanning calorimetry (DSC). We summarize the characterization results of embedded nanoparticles in Fig.3. Fenofibrate nanoparticles in the beads are present in crystalline form since the PXRD pattern is consistent with the standard pattern of fenofibrate crystals (Fig.3 (a)). Naturally, it is also important to understand and control the crystal size of the API as it greatly influences the dissolution kinetics. We show in our previous work that fenofibrate crystal size is dictated by the nanoemulsion droplet size and and is approximately equal to the initial droplet size [22, 23]. This is corroborated by DSC results where we observe a decrease in melting point from 79 °C to 67 °C with changes in nanoemulsion droplet size from 650 nm to 220 nm (Fig.3 (b)). This is consistent with the prior reports in literature where DSC measurements show that the melting point of fenofibrate decreases with decrease of API nanocrystal size [33]. In addition, the amount of embedded fenofibrate nanocrystals (% drug loading on dry basis) can also be tuned by varying the SOR. The drug loading capacity increases from 32% to 50% when the SOR decrease from 2.0 to 0.25 (see the Supporting Information).

In contrast to fenofibrate, we find that ibuprofen nanoparticles do not show an XRD pattern consistent with standard ibuprofen crystals (Fig.3 (c)). This implies that ibuprofen particles are present in an amorphous state. DSC results further confirm the amorphous form of embedded nanoparticles (Fig.3 (d)), as we do not see any endothermic peak at 78 °C - a characteristic of the melting of the bulk phase of ibuprofen [33]. The loss of crystalline nature of ibuprofen may be explained by the molecular interaction between ionized ibuprofen and the alginate, which may induce the formation of nanoconjugates by disrupting the crystal lattice of ibuprofen [34]. Previous studies show that the API-polymer interactions due to ionic or intermolecular H-bonding interactions stabilize solid dispersions and prevent re-crystallization during dissolution [35]. It should be noted that amorphous form of a poorly soluble API has higher

This article is protected by copyright. All rights reserved.

Author Manuscript

apparent solubility and improved dissolution rate as compared to its crystalline form since no crystal lattice has to be broken down for dissolution to take place [36, 37]. Though the amorphous form of APIs represents another promising technique to improve the bioavailability of poorly water-soluble drugs, their stabilization is a major concern [35, 38]. However, in this study, the ibuprofen amorphous particles encapsulated inside the ionic polymer (alginate) hydrogel matrix remain stable at least four months at 25°C and 60% relative humidity (see the DSC/ XRD results in the Supporting Information). We also observe that with the change of SOR (from 0.25 to 2.0) the formulated products do not show any crystallinity or any transformation from amorphous state to crystalline state. The porous nano-confinement environment within the alginate hydrogel matrix is believed to prevent re-crystallization of the homogeneously dispersed ibuprofen drug molecules. Recently, micro- or meso-porous materials such as, SBA-15, MCM-41, controlled porous glass (CPG), that exploit their nano-space confinement and surface chemistry, have been used for amorphization of poorly water-soluble drugs with long-term storage stability [39–41]. Moreover, we can increase the drug loading capacity up to 30% with a decrease of SOR to 0.25 (Supporting Information). Unlike the fenofibrate nanoparticles, the ibuprofen particle size is not the same as that of the nanoemulsion droplet size, probably because of being in the amorphous state, and the saturation solubility difference between fenofibrate and ibuprofen in the dispersed phase (anisole). It is also observed that the loading capacity of ibuprofen (21%) is lower than that of fenofibrate (39%) at a fixed oil weight fraction (15%) due to their solubility difference in anisole. Typically, the embedded ibuprofen amorphous nanoparticles are found to be 40-60% of the original nanoemulsion droplet size (see Fig.S3 in the Supporting Information).

3.2 Dissolution Results

Fig.4 provides a summary of dissolution profiles profiles of fenofibrate and ibuprofen from different formulations. We independently vary the hydrogel bead size (radius: R_b) as well as the API nanoparticle size (radius: R_c), and measure relative concentration of drug(s) in bulk (θ_∞) with time. Increasing R_b and / or R_c slows down the dissolution rate for fenofibrate nanocrystals (Fig.4 (a), (b)). Increasing R_b from 50 μm to 500 μm changes t_{70} from 12.5 min to 100 min and increasing R_c from 165 nm to 650 nm changes t_{70} from 12.5 min to 45 min (t_{70} is the time to reach $\theta_\infty = 0.7$). Similar to fenofibrate, for ibuprofen, increasing the value of R_b from 50 μm to 550 μm, changes t_{70} from 3.7 min to 33.3 min. These dissolution rates are comparable and in some cases even faster than those reported in literature [22, 33, 40, 42, 43]. For example, Dwyer *et al.* showed that fenofibrate nanocrystals prepared from the 70-nm CPG matrix achieve $t_{80} = 42$ min [33]. In addition, the dissolution kinetics of our fenofibrate nanocrystal formulations is also comparable to that of the-state-of-the-art fenofibrate formulation commercialized as TriCor tablets which are prepared by a nano-milling technique [22]. Shen *et al.* reported that amorphous ibuprofen prepared from co-sprayed solid dispersion with SBA-15 have $t_{95} = 15$ min whereas commercial ibuprofen only shows $\theta_\infty = 0.16$ in the same time frame [39]. Zhang *et al.* found $t_{80} = 60$ min for amorphous ibuprofen dissolution from mesoporous Mg-carbonate [42]. Though the above-mentioned studies show similar dissolution rates to the ones we report, our ability to access a wide range of R_b and R_c, and vary both parameters independently, provides us with flexibility to control the dissolution profile. We now use an order of magnitude analysis to develop a physical picture of the complete dissolution process and to estimate the importance of different physical parameters.

Results from our theoretical analysis are summarized in Fig.5. We assume that both drug nanoparticles and beads are spherical with radius R_c (initial radius) and R_b respectively (Fig.5 (a)). Since the nanoparticles dissolve, their size varies with time, denoted here by $R_c'(t)$. We also assume that drug nanoparticles are distributed uniformly throughout the bead. We can expect the concentration of dissolved drug in the bead to evolve over time, as shown in Fig.5 (b). Initially, the concentration of drug is uniform inside the bead but as the time goes on, concentration decays radially outwards. This happens because the drug will first dissolve at the radially outermost layer of nanoparticles and then move inwards. Therefore, at any given time, the concentration only decays between $R_b'(t) < r < R_b$, where R_b' is the radial distance below which the drug concentration is uniform. Naturally, at $t = 0$, $R_b'(0) = R_b$, or the concentration is uniform throughout the entire bead. For the sake of simplicity, we only perform an order of magnitude analysis. We note that at any given time t, the drug dissolves from the nanoparticles between $R_b'(t) < r < R_b$, diffuses radially outwards in the bead, and then dissolves in the bulk. The drug dissolution and diffusion step can be described as:

$$N_{NP} = k(C_{\text{sat}} - C)4\pi R_c(t)^2 \tag{1}$$

where N_{NP} is the amount of drug diffusing out per unit time from a single nanoparticle, k is the mass transfer coefficient, C_{sat} is the saturated concentration of the drug in the bead, and C is the concentration of the drug just outside the nanoparticle. Since there is no flow within the bead, mass transfer coefficient is given by $k \sim \frac{D}{\delta}$, where

This article is protected by copyright. All rights reserved.

Author Manuscript

Author Manuscript

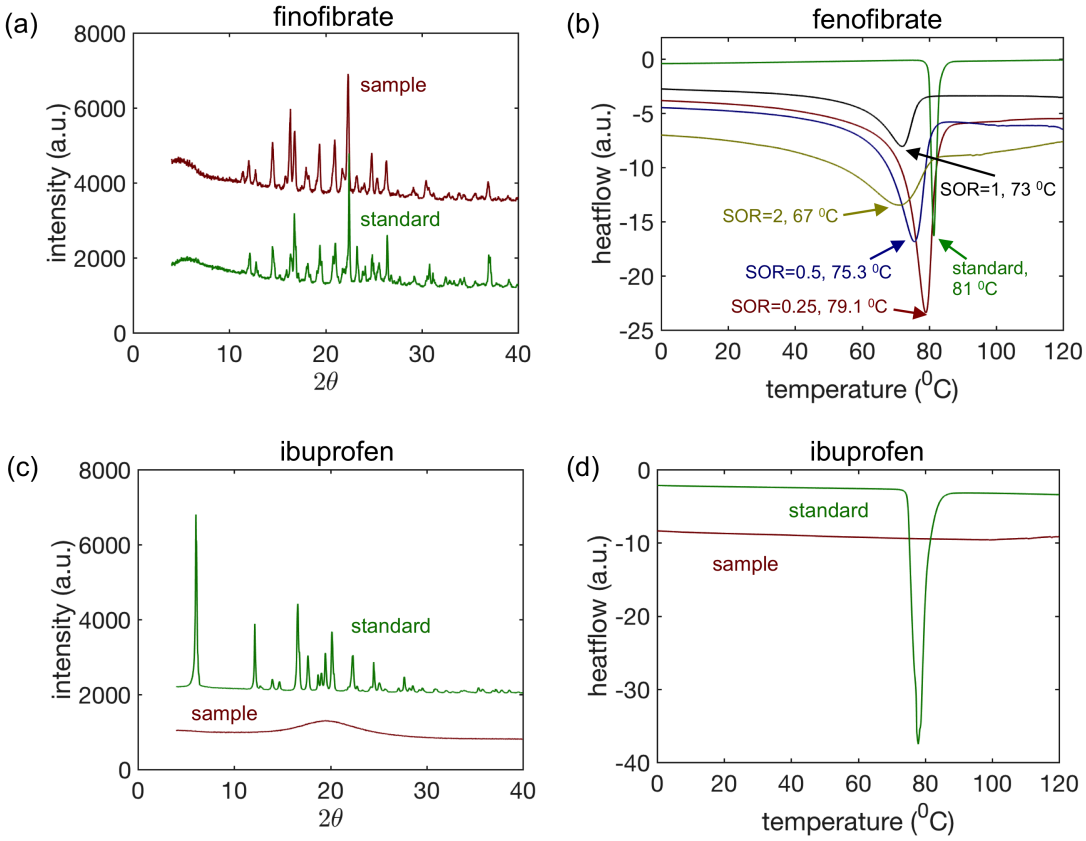

Figure 3: **Characterization of fenofibrate and ibuprofen nanoparticles embedded inside hydrogel beads.** (a) Powder X-ray diffraction (PXRD) data suggests that fenofibrate is present in crystalline form since the pattern from standard fenofibrate crystal is consistent with the pattern from nanoparticle embedded inside hydrogel beads. (b) Differential scanning calorimetry (DSC) data shows the effects of SOR (used in the formulation step) on the melting point of fenofibrate particles. The nanoemulsion droplet size changes from 650 nm (SOR=0.25) to 220 nm (SOR=2) and their corresponding melting points changes from 79°C to 67°C. (c) PXRD data suggests that ibuprofen particles are present in amorphous form since patterns from ibuprofen nanoparticles are not consistent with data from a standard crystal. (d) DSC data corroborates finding in (c) since no melting point is observed for ibuprofen nanoparticles.

This article is protected by copyright. All rights reserved.

Author Manuscript

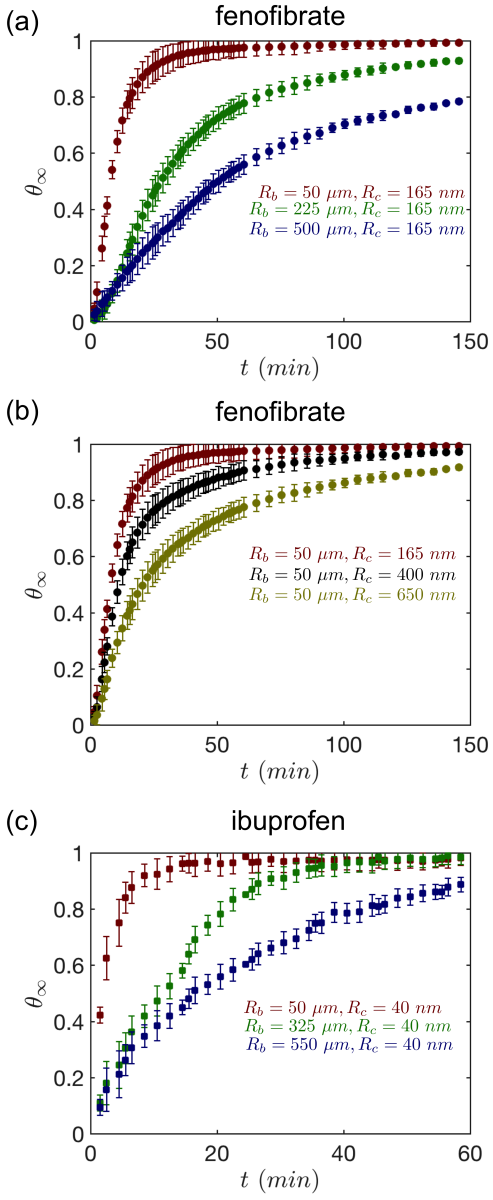

Figure 4: **Dissolution profiles for different R_b and R_c.** (a) Evolution of θ_∞ for fenofibrate crystals in alginate beads for different values of R_b keeping R_c constant. We observe that increasing R_b slows down the dissolution rate. (b) Evolution of θ_∞ for fenofibrate crystals in alginate beads for different values of R_c keeping R_b constant. Similar to R_b, increase in R_c slows down the dissolution rate. (c) Evolution of θ_∞ for ibuprofen particles where similar to fenofibrate, increase in R_b slows down the dissolution rate.

This article is protected by copyright. All rights reserved.

δ is the boundary layer thickness, or the thickness where concentration changes. Based on our physical picture in Fig.5, $\delta \sim R_b - R_b'(t)$, and δ varies with time. However, for an order of magnitude estimate, we can assume $\delta \sim R_b$ and $k \sim D/R_b$. Similarly, $C_{\text{sat}} - C$ is a function of position as well as time. However, as a first approximation, we can assume $C_{\text{sat}} - C \sim C_{\text{sat}}$. We also note that the nanoparticle radius $R_c'(t)$ is not a constant and ultimately vanishes. However, the relevant scale of $R_c'(t)$ is the initial radius $R_c'(t) \sim R_c$. We can estimate the order of magnitude value of N_{NP} from Equation (1) as (neglecting numerical prefactors):

$$N_{NP} \sim \frac{D}{R_b} C_{\text{sat}} R_c^2 \tag{2}$$

Now, we estimate the amount of drug dissolving into the bulk solution from all beads. The number of nanoparticles dissolving per bead in a given time t is:

$$n_{NP,B} \sim \frac{\phi \rho_b (R_b^3 - R_b'(t)^3)}{\rho_c R_c^3} \sim \frac{\phi \rho_b R_b^3}{\rho_c R_c^3} \tag{3}$$

where ϕ is the fraction of drug inside the bead (either by weight or mole), ρ_b is the density of the alginate bead, and ρ_c is the density of the nanoparticle. We note that for a given time t, the nanoparticles would only be dissolving between $R_b'(t) < r < R_b$. As before, we approximate $R_b^3 - R_b'(t)^3 \sim R_b^3$. Now, the total number of beads in bulk for a fixed amount of alginate m_b is:

$$n_B \sim \frac{m_b}{\frac{4\pi}{3} \rho_b R_b^3} \tag{4}$$

Therefore, the amount of drug dissolving from all beads is (neglecting numerical prefactors):

$$N_{\text{total}} \sim n_B n_{NP,B} N_{NP} \sim \frac{m_b \phi D C_{\text{sat}}}{\rho_c R_b R_c} \tag{5}$$

Since N_{total} is the amount of drug uptake in the bulk, it can also be estimated as:

$$N_{\text{total}} \sim V \frac{dC_\infty}{dt} \sim V \frac{C_\infty}{t} \tag{6}$$

where V is the volume of bulk solution, C_∞ is the concentration of drug in bulk, and t is time. Comparing the two estimates:

$$\frac{V C_\infty}{t} \sim \frac{m_b \phi D C_{\text{sat}}}{\rho_c R_b R_c} \tag{7}$$

or:

$$\frac{C_\infty}{\frac{m_b \phi}{V}} \sim \frac{D C_{\text{sat}} t}{\rho_c R_b R_c} \tag{8}$$

or

$$\theta_\infty \sim \tilde{t} \tag{9}$$

where $\theta_\infty = \dfrac{C_\infty}{\frac{m_b \phi}{V}}$ is the relative amount of drug dissolved in the bulk and $\tilde{t} = \dfrac{D C_{\text{sat}} t}{\rho_c R_b R_c}$ is a dimensionless time scale. According to our calculations, all of our data for various concentrations (θ_∞) should collapse when plotting against $\tilde{t}$. We re-plot the data presented in Fig.4 by scaling the time t as $\tilde{t} = \dfrac{D C_{\text{sat}} t}{\rho_c R_b R_c} = \dfrac{\beta t}{R_b R_c}$ where we fit the value of β for fenofibrate as well as ibuprofen such that the scale of $\tilde{t}$ is of the order of unity. The values of β used for fenofibrate and ibuprofen are 4.25×10^{-15} m^2/s and 7.5×10^{-15} m^2/s respectively (a discussion on the fitted values of β and their significance is provided in the Supporting Information). R_b, R_c are taken from experiments. The results are provided in Fig.5 (b, c). The results clearly show that we are able to collapse the data on a master curve. This is especially promising since we collapse the entire dissolution profile, unlike recent reports [22, 23]. We also note that the collapse of experimental data onto a single curve is independent of the fitting parameter β since the value of β is kept constant across different data sets. Overall, our model provides useful information about the dissolution kinetics. For instance, since the system is governed by $\tilde{t}$, we know that increasing R_b by a factor of 10 will increase dissolution time by 10-fold. Similarly, if we increase R_c by 10 times, dissolution time will increase by 10-fold. Since we only perform an order of magnitude analysis and neglect effects such as re-hydration of the alginate bead, our current analysis is only a first-order approximation. However, the analysis still provides critical information about parameters governing the physical process.

Author Manuscript

This article is protected by copyright. All rights reserved.

Author Manuscript

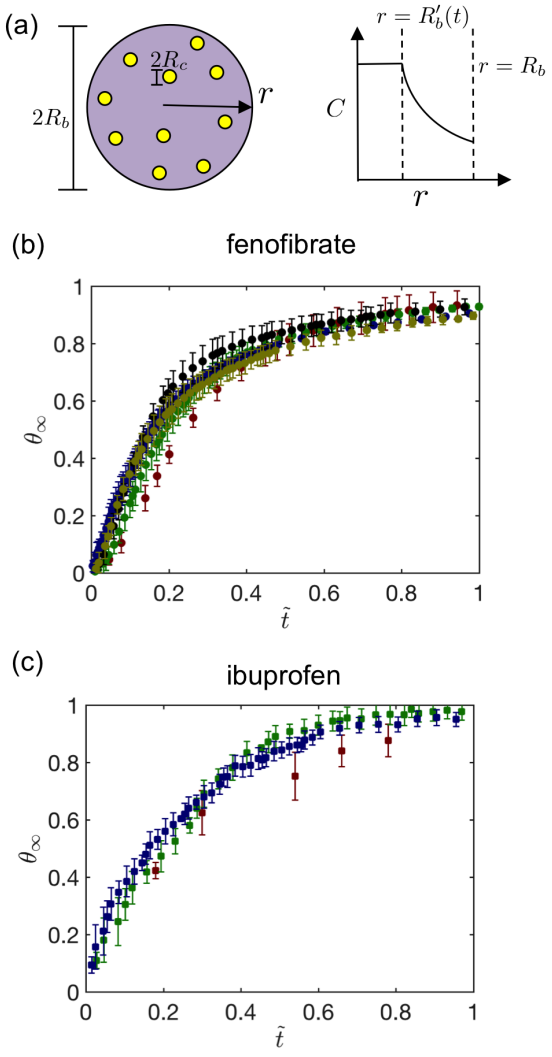

Figure 5: **Physical model and collapse of dissolution data.** (a) Schematic of our physical model that assumes spherical nanoparticles with radius R_c are uniformly distributed in the bead with radius R_b. The concentration decays between $R_b'(t) < r < R_b$. Initially, $R_b'(0) = R_b$. Upon re-scaling the variation of θ_∞ with $\tilde{t}$, we are able to collapse entire dissolution data for (b) fenofibrate and (c) ibuprofen. $\tilde{t} = \dfrac{\beta t}{R_b R_c}$ where we fit the value of β. The values of β used for fenofibrate and ibuprofen are 4.25×10^{-15} m^2/s and 7.5×10^{-15} m^2/s respectively.

This article is protected by copyright. All rights reserved.

3.3 Co-formulation of drugs

As discussed in Fig.1, using a mixture of two or more nanoemulsion provides a route to embed multiple drugs inside a single polymer matrix (*i.e.* co-formulation). We note that it is also possible to separately mix the beads containing different APIs. However, it is preferred to have them inside a single matrix since that opens up the possibility to exploit synergy effects [44–46]. Moreover, it is easier to mix nanoemulsions prior to bead generation as compared to generating different sized beads, thus adding the dosing compliance. Fig.6 shows the *in vitro* dissolution properties of co-formulation of fenofibrate nanocrystals ($\sim$ 500 nm in diameter) and ibuprofen amorphous nanoparticles ($\sim$ 80 nm in diameter) contained in a hydrogel bead of 100 μm in diameter. The dissolution kinetics results are consistent with the trends obtained for APIs reported in Fig.4, suggesting that there is no detrimental effect on dissolution due to the presence of multiple drugs. To vary the release profiles of both ibuprofen and fenofibrate, we can vary the bead size. However, to vary the dissolution profile of an individual drug, we can tune the nanoparticle size by varying any formulation parameter. Thus the flexibility of our approach offers the possibility to design dosages of multiple hydrophobic drugs with future tailor-made controlled release formulations. In addition, hydrogels loaded with multiple drugs could reduce the frequency of drug administration, potentially facilitating the patient compliance.

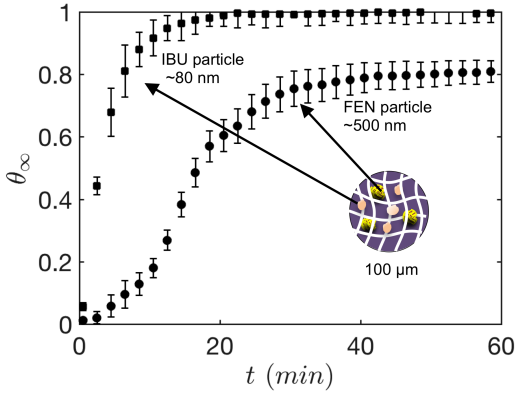

Figure 6: **Demonstration of co-formulation.** Dissolution data where both fenofibrate crystals and ibuprofen particles were incorporated in a single bead. The beads were created by dripping a mixture of two nanoemulsions where one carried fenofibrate in the dispersed phase and the other carried ibuprofen in the dispersed phase.

4 Conclusion and Outlook

We present here a low-energy method to make composite hydrogel beads encapsulated with single and multiple hydrophobic drugs. Characterization of the API particles embedded inside the hydrogels by SEM, DSC and PXRD proved that both embedded fenofibrate and ibuprofen particles are in nanometer size range, and crystalline and amorphous in nature, respectively. Since our bottom-up formulation approach only requires simple unit operations such as mixing and dripping, there is significant potential to adapt this technique at an industrial scale. Further, due to our ability to control the size of both API particles and hydrogel beads, we can adjust the time of drug release profile anywhere from 10 - 200 min. This is particularly useful since it might be desirable to have a faster dissolution of a particular drug and a slower release of another, or to have faster release of both drugs to optimize the therapeutic efficacy. In fact reports indicate an increasing demand in dosage forms that carry multiple APIs in fixed dose combination [38, 47]. We also build a physical model that successfully explains the dependence of release rate on API nanoparticle size and hydrogel bead size, providing us with a rationale to design systems. Since the model is mechanistic in nature, the learning can also be extended to different APIs and hydrogel chemistry. Lastly, our composite hydrogels with adjustable drug loading capacity also have a potential to be served as final solid dosage forms (tablets, capsules) for oral delivery.

Acknowledgement

A.Z.M Badruddoza and A.Gupta contributed equally to this work. The authors acknowledge the Novartis-MIT Center for Continuous Manufacturing for financial support and use of instrumentation (differential scanning calorimetry

This article is protected by copyright. All rights reserved.

Author Manuscript

(DSC), X-ray diffraction (XRD) and dissolution (USP II) apparatus). A. Gupta is grateful for financial support from the Hugh Hampton Young Fellowship.

References

[1] T. Takagi, C. Ramachandran, M. Bermejo, S. Yamashita, L. X. Yu, G. L. Amidon. *Mol. Pharmaceutics* **2006**, *3*, 6 631.

[2] K. Göke, T. Lorenz, A. Repanas, F. Schneider, D. Steiner, K. Baumann, H. Bunjes, A. Dietzel, J. H. Finke, B. Glasmacher, et al. *Eur. J. Pharm. Biopharm.* **2017**.

[3] L. Gao, D. Zhang, M. Chen. *J. Nanopart. Res.* **2008**, *10*, 5 845.

[4] M. E. Brewster, T. Loftsson. *Adv. Drug Delivery Rev.* **2007**, *59*, 7 645.

[5] H. Chen, C. Khemtong, X. Yang, X. Chang, J. Gao. *Drug Discovery Today* **2011**, *16*, 7 354.

[6] Y. Kawabata, K. Wada, M. Nakatani, S. Yamada, S. Onoue. *Int. J. Pharm.* **2011**, *420*, 1 1.

[7] R. Müller, S. Schmidt, I. Buttle, A. Akkar, J. Schmitt, S. Brömer. *Int. J. Pharm.* **2004**, *269*, 2 293.

[8] J.-U. A. Junghanns, R. H. Müller. *Int. J. Nanomed.* **2008**, *3*, 3 295.

[9] Y. Singh, J. G. Meher, K. Raval, F. A. Khan, M. Chaurasia, N. K. Jain, M. K. Chourasia. *J. Controlled Release* **2017**, *252* 28.

[10] A. A. Date, N. Desai, R. Dixit, M. Nagarsenker. *Nanomedicine* **2010**, *5*, 10 1595.

[11] A. Gupta, H. B. Eral, T. A. Hatton, P. S. Doyle. *Soft Matter* **2016**, *12*, 11 2826.

[12] T. G. Mason, J. Wilking, K. Meleson, C. Chang, S. Graves. *Journal of Physics: Condensed Matter* **2006**, *18*, 41 R635.

[13] T. Tadros, P. Izquierdo, J. Esquena, C. Solans. *Adv. Colloid Interface Sci.* **2004**, *108* 303.

[14] C. Solans, P. Izquierdo, J. Nolla, N. Azemar, M. Garcia-Celma. *Curr. Opin. Colloid Interface Sci.* **2005**, *10*, 3 102.

[15] A. Gupta, H. B. Eral, T. A. Hatton, P. S. Doyle. *Soft Matter* **2016**, *12*, 5 1452.

[16] A. Gupta, V. Narsimhan, T. A. Hatton, P. S. Doyle. *Langmuir* **2016**, *32*, 44 11551.

[17] M. M. Fryd, T. G. Mason. *Annu. Rev. Phys. Chem.* **2012**, *63* 493.

[18] A. Gupta, A. Z. M. Badruddoza, P. S. Doyle. *Langmuir* **2017**, *33*, 28 7118.

[19] H. Z. An, M. E. Helgeson, P. S. Doyle. *Adv. Mater.* **2012**, *24*, 28 3838.

[20] D. Jagadeesan, I. Nasimova, I. Gourevich, S. Starodubtsev, E. Kumacheva. *Macromol. Biosci.* **2011**, *11*, 7 889.

[21] D. J. McClements. *Annu. Rev. Food Sci. Technol.* **2010**, *1* 241.

[22] H. B. Eral, M. OMahony, R. Shaw, B. L. Trout, A. S. Myerson, P. S. Doyle. *Chem. Mater.* **2014**, *26*, 21 6213.

[23] A. Z. M. Badruddoza, P. D. Godfrin, A. S. Myerson, B. L. Trout, P. S. Doyle. *Adv. Healthcare Mater.* **2016**, *5*, 15 1960.

[24] G. Vergote, C. Vervaet, I. Van Driessche, S. Hoste, S. De Smedt, J. Demeester, R. Jain, S. Ruddy, J. P. Remon. *Int. J. Pharm.* **2001**, *219*, 1 81.

[25] R. A. Leon, W. Y. Wan, A. Z. M. Badruddoza, T. A. Hatton, S. A. Khan. *Cryst. Growth Des.* **2013**, *14*, 1 140.

[26] A. I. Toldy, A. Z. M. Badruddoza, L. Zheng, T. A. Hatton, R. Gunawan, R. Rajagopalan, S. A. Khan. *Cryst. Growth Des.* **2012**, *12*, 8 3977.

Author Manuscript

This article is protected by copyright. All rights reserved.

[27] R. A. Leon, A. Z. M. Badruddoza, L. Zheng, E. W. Yeap, A. I. Toldy, K. Y. Wong, T. A. Hatton, S. A. Khan. *Cryst. Growth Des.* **2014**, *15*, 1 212.

[28] J. Siepmann, N. Peppas. *Adv. Drug Delivery Rev.* **2012**, *64* 163.

[29] P. L. Ritger, N. A. Peppas. *J. Controlled Release* **1987**, *5*, 1 37.

[30] S. Jamzad, R. Fassihi. *AAPS PharmSciTech* **2006**, *7*, 2 E17.

[31] B. Sütő, S. Berkó, G. Kozma, Á. Kukovecz, M. Budai-Szűcs, G. Erős, L. Kemény, A. Sztojkov-Ivanov, R. Gáspár, E. Csányi. *Int. J. Nanomed.* **2016**, *11* 1201.

[32] H. B. Eral, E. R. Safai, B. Keshavarz, J. J. Kim, J. Lee, P. Doyle. *Langmuir* **2016**, *32*, 28 7198.

[33] L. Dwyer, V. Michaelis, M. O'Mahony, R. Griffin, A. Myerson. *CrystEngComm* **2015**, *17*, 41 7922.

[34] A. O. Abioye, A. Kola-Mustapha. *Pharm. Res.* **2015**, *32*, 6 2110.

[35] P. Kanaujia, P. Poovizhi, W. Ng, R. Tan. *Powder Technol.* **2015**, *285* 2.

[36] C. Goddeeris, T. Willems, G. Van den Mooter. *Eur. J. Pharm. Sci.* **2008**, *34*, 4 293.

[37] R. Laitinen, K. Löbmann, C. J. Strachan, H. Grohganz, T. Rades. *Int. J. Pharm.* **2013**, *453*, 1 65.

[38] A. Alhalaweh, C. A. Bergström, L. S. Taylor. *J. Controlled Release* **2016**, *229* 172.

[39] S.-C. Shen, W. K. Ng, L. Chia, J. Hu, R. B. Tan. *Int. J. Pharm.* **2011**, *410*, 1 188.

[40] S.-C. Shen, W. K. Ng, L. Chia, Y.-C. Dong, R. B. Tan. *J. Pharm. Sci.* **2010**, *99*, 4 1997.

[41] G. Rengarajan, D. Enke, M. Steinhart, M. Beiner. *J. Pharm. Sci.* **2008**, *18*, 22 2537.

[42] P. Zhang, J. Forsgren, M. Strømme. *Int. J. Pharm.* **2014**, *472*, 1 185.

[43] T. Numpilai, S. Muenmee, T. Witoon. *Mater. Sci. Eng. C* **2016**, *59* 43.

[44] G. Pelaia, R. Maselli, L. Gallelli. *Multidisciplinary Respiratory Medicine* **2014**, *9*, 1 64.

[45] T. Taupitz, J. B. Dressman, S. Klein. *Eur. J. Pharm. Biopharm.* **2013**, *84*, 1 208.

[46] R. A. Leon, A. Somasundar, A. Z. M. Badruddoza, S. A. Khan. *Part. Part. Syst. Charact.* **2015**, *32*, 5 567.

[47] K. Letchmanan, S.-C. Shen, W. K. Ng, R. B. Tan. *Colloids Surf. B* **2017**, *155* 560.

Author Manuscript

This article is protected by copyright. All rights reserved.